A novel method for accurate extraction of liver capsule and auxiliary diagnosis of liver cirrhosis based on high-frequency ultrasound images

Yiwen Liu [a], Xiang Liu [a,*], Shuohong Wang [b], Jialin Song [c], Jianquan Zhang [c]

[a] School of Electric and Electronic Engineering, Shanghai University of Engineering Science, Shanghai, 201620, China
[b] Department of Molecular and Cellular Biology and Center for Brain Science, Harvard University, Cambridge, USA
[c] Department of Ultrasound, Changzheng Hospital Affiliated to Second Military Medical University, Shanghai, 200001, China

ABSTRACT

Liver cirrhosis is a common chronic progressive disease with a high mortality rate. The early diagnosis and treatment of liver cirrhosis is an important research subject in the medical field. In this paper, a novel method is proposed for the accurate extraction of the liver capsule and auxiliary diagnosis of cirrhosis based on high frequency ultrasound images. First, a self-developed method is used to extract the predictive capsule of ultrasound images, which involves the detection of liver ascites with sliding windows, image enhancement with multiscale detail and fuzzy set, structure segmentation with morphological processing, and predictive capsule detection with traversal search method. Thereafter, the real capsule is obtained by the gray difference method according to different gray values between the liver capsule region of the original ultrasound images and the set threshold. Finally, according to the analysis of smoothness, as well as the continuity and fluctuation of predictive and real capsule, four novel features called *NoL, VoS, CV,* and *NoF* are proposed for the computer auxiliary diagnosis model. This model is designed on the basis of support vector machine and k-means clustering and can classify normal liver and three liver cirrhosis stages. The experimental results reveal that the accuracy of the liver capsule extraction using this model is 95.13% and final classification accuracy of four stages can reach 92.54%, 88.46%, 89.23% and 94.55%, respectively. The results also indicate that the method proposed in this paper can achieve the classification of liver cirrhosis stages much more accurately and efficiently compared with previously utilized methods.

1. Introduction

Liver cirrhosis is a common chronic progressive disease which is specifically defined as the histological development of a fiber band around the regeneration nodule caused by a chronic liver injury. As liver cirrhosis progresses, portal hypertension and end-stage liver disease can be caused, which has higher mortality. Therefore, the early detection and treatment of liver cirrhosis is important [1]. Currently, the cirrhosis diagnosis mainly depends on the subjective judgement of the doctor. Because of the influence of experience or other factors, there may be a significant difference in the diagnosis results among individuals. Therefore, a computer-assisted diagnosis system of liver cirrhosis based on quantitative analysis is necessary. An accurate and high-efficiency computer-assisted diagnosis system can be applied in a clinic for assisting doctors to obtain accurate diagnosis and treatment with different stages of liver cirrhosis.

Ultrasound imaging is an imaging technique based on the physical properties of ultrasound and the parameters of human histology. During medical auxiliary diagnosis, ultrasound technology is often the preferred method of imaging examination [2,3], as it processes the characteristics of non-ionizing radiation, easy operation and cheap price. Moreover, high-frequency ultrasound imaging is more suitable for liver detection and diagnosis, as it provides high-resolution output. The images obtained by high-frequency ultrasound showed grain texture [4], which could sensitively detect the size, shape, edge, echo of liver parenchyma, and abnormal changes in the intrahepatic bile duct and blood vessels, thereby ensuring that the lesions could be detected and treated in time. For a normal liver, the capsule is a linear structure with continuous, smooth, and uniform thickness. With the development of liver cirrhosis, the parenchyma of a liver begins aging gradually, which leads to an
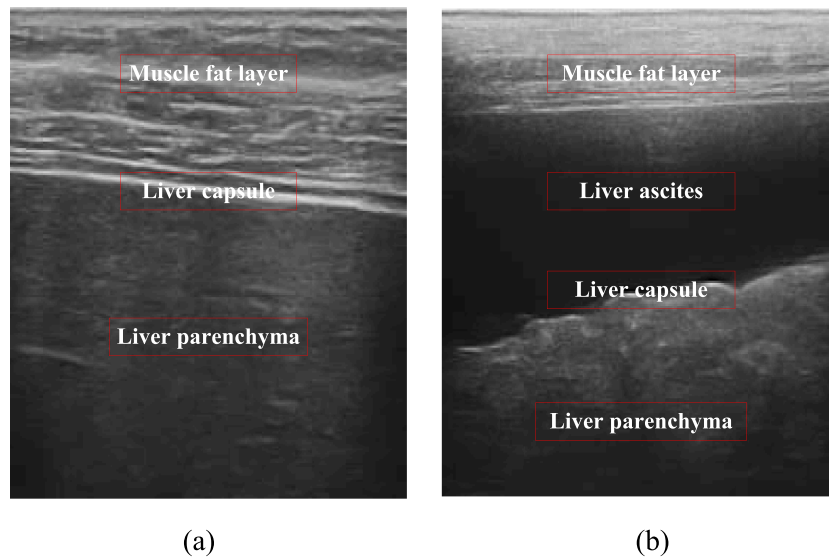

Fig. 1. Introduction of ultrasound image structure
(a) No-ascites image, (b)
Ascites image.

abnormal appearance of the outline of the liver capsule. The liver capsule becomes uneven, usually appearing wavy, ladder-like or serrated [5], and even broken.

These existing computer-assisted diagnosis methods of liver cirrhosis based on ultrasound images mainly involve the study of the liver parenchyma and liver capsule. The related research on liver parenchyma mainly extracts the texture features of liver parenchyma [6] such as fractal, statistical texture, spectral, and combined features to quantitatively analyze the parenchymal structure in liver ultrasound images. Moreover, various classifiers such as random forests, support vector machine (SVM) and neural networks have been used to classify different liver cirrhosis stages. Xu et al. [7] employed the residual network to identify the liver parenchyma in order to achieve staging identification of cirrhosis after the isolation of liver parenchyma. Although they achieved good results, they required a substantial amount of data to train the model. From the perspective of clinical medicine, the direct use of deep learning techniques cannot obtain specific features consistent with actual observations. It is impossible to predict the worst result from the use of such techniques and the reason for its recognition errors.

Further, changes in the morphological characteristics of the liver capsule are also important indicators in clinical diagnosis. Liu et al. [8] extracted the liver capsule by combining vertical gradient optimization and minimum deflection error and proposed three morphological features to describe the liver capsule. Wang et al. [5] identified the location of the liver capsule by utilizing a multi-scale and multi-objective optimization algorithm, and proposed indices to measure the continuity and smoothness. The SVM was used to identify the stage of liver cirrhosis by combining the features of liver parenchyma and capsule. However, the effect of this method on mild and severe classification is not ideal because it is too sensitive to subtle changes. Liu et al. [9] proposed the use of dynamic programming and neural networks to extract the liver capsule and its characteristics and identified the stage of liver cirrhosis by utilizing SVM. However, this method relies on the manual initialization of the liver capsule and its efficiency is relatively low. Zhao et al. [10] extracted the boundary of the liver capsule by a spatial context-constrained multi-scale method and proposed two novel geometric features of the liver capsule were proposed to classify the cirrhosis. This method causes a false extraction of the severely broken liver capsule and has a low recognition rate for the mild and moderate stages. Fu et al. [11] proposed a new method for extracting the liver capsule by combining the recognition of ascites in liver ultrasound

images and dynamic programming. It is possible to effectively avoid the missing the detection of the liver capsule, but it is not ideal for classification of moderate and severe stages in the case of fracture and fluctuation.

In order to improve the accuracy of liver capsule extraction and cirrhosis auxiliary diagnosis, a novel method of extracting and quantifying the liver capsule based on a high-frequency ultrasonic image is proposed in this paper. The main contributions of this paper are summarized in the following manner: 1) a liver capsule extraction method is designed that can automatically and accurately achieve the extraction of predictive and real liver capsule; 2) four novel morphological indexes are proposed for the predictive and real liver capsule, which can provide a more comprehensive description of morphological changes in the liver capsule; 3) a two-stage classification model is designed, which can accurately and effectively classify four different stages.

The remainder of this paper is organized in the following manner. The materials and methods are described in detail in Section 2. The results and discussion are presented in Section 3. The paper is concluded in Section 4.

2. Materials and methods

2.1. Patients and system building

The data set utilized in this paper was provided by the department of ultrasound, Changzheng Hospital Affiliated to Second Military Medical University. The data set included 47 patients with HBV Cirrhosis, including 35 males and 12 females, aged between 28 and 77 years old, as well as 20 randomly selected patients without liver disease, including 15 males and 5 females, aged between 26 and 76 years old. The wide age range of healthy controls was selected in order to be consistent with the age range of patients with liver cirrhosis. Meanwhile, the absence of liver disease among patients was confirmed through physical examination, laboratory examination (including blood examination), ultrasound, or other imaging examination. According to Child-Pugh improved classification standards, patients with cirrhosis can be classified into three groups: mild, moderate and severe. In our data set, there were 18 cases of mild cirrhosis, aged between 31 and 71 years old; 16 cases of moderate cirrhosis, aged between 28 and 67 years old; and 13 cases of severe cirrhosis including 8 cases with ascites, aged between 33 and 77 years old. This was also confirmed by laboratory examination,
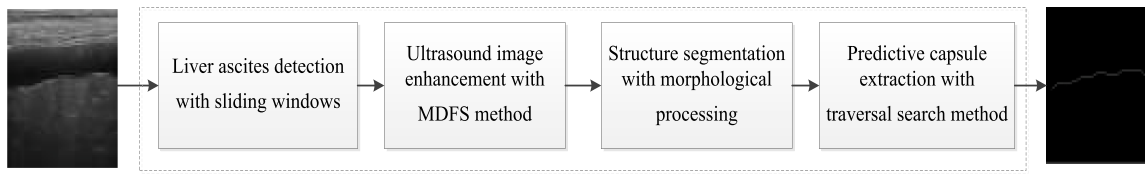
Fig. 2. Flow chart of PLCD method.

ultrasound, or computed tomography (CT) examination. Moreover, none of the participants had received anti-fibrosis treatment. There are no significant differences in age, sex, and physique among the patients in both groups.

The Voluson E8 ultrasound machine (GE Medical Systems, USA) with a scanning-probe system, with a frequency of between 4 MHz and 10 MHz was used in this experiment. Liver tissue was scanned using the xiphoid process and right intercostal space respectively when the patients were in supine position or left decubitus position, respectively. The two-dimensional images of the left and right hepatic lobe capsule were obtained and used for the algorithm design of computer auxiliary diagnosis on Matlab 2016b.

The auxiliary diagnosis system of cirrhosis stages via the novel method of extracting and quantifying the liver capsule based on morphological features that is proposed in this paper can be divided into four main aspects: 1) predictive capsule extraction; 2) real liver capsule extraction; 3) morphological analysis; 4) design of stage diagnosis model.

2.2. Detection of the predictive capsule using the PLCD method

Cirrhosis is a common diffuse liver injury disease in modern society. The disease can be divided into three stages: mild, moderate, and severe. It is evident from Fig. 1 that the structure of the liver ultrasound image is complicated, mainly comprising of muscle fat layer, liver capsule, and liver parenchyma. In severe cirrhosis cases, liver ascites may be found. In order to identify the structural differences among these ultrasound images, the image processing technology is applied to the ultrasound images. The capsule that is directly extracted from these images is defined as the "prediction capsule". The predicted capsule can overcome the problem of insufficient extraction of the liver capsule when it is severely broken. This does not only encompass the provision of the location information of the capsule in an actual case but can also reflect the overall trend of the liver capsule.

In this paper, a novel predictive liver capsule detection (PLCD) method is proposed, which consists of four parts: ascites image judgment, image enhancement, morphological processing, and predictive liver capsule extraction. The flow chart is presented in Fig. 2.

2.2.1. Detection of liver ascites with sliding windows

Liver ascites is an ascitic syndrome caused by liver function damage and portal hypertension in the later stage of cirrhosis [12]. Due to the presence of ascites, the structure of the entire liver in an ultrasound image shows as change; this implies that the ultrasound images can be divided into two major categories of ascites and without ascites. In order to detect the liver capsule more effectively and accurately, different processing parameters must be set for the two types of images. Therefore, it is necessary to judge whether the captured liver ultrasound images contain ascites.

Normally, the liver ascites area has a low gray value and is mainly concentrated in the upper portion of the ultrasound images. In this paper, the existence of ascites is detected by the sliding window method [13]. We conduct an experiment in which a sliding window of $L \times L$ is designed, which slides from left to right and top to bottom in the upper portion of ultrasound images with a stride of one pixel to fully traverse the upper portion of the entire image. The schematic diagram of the
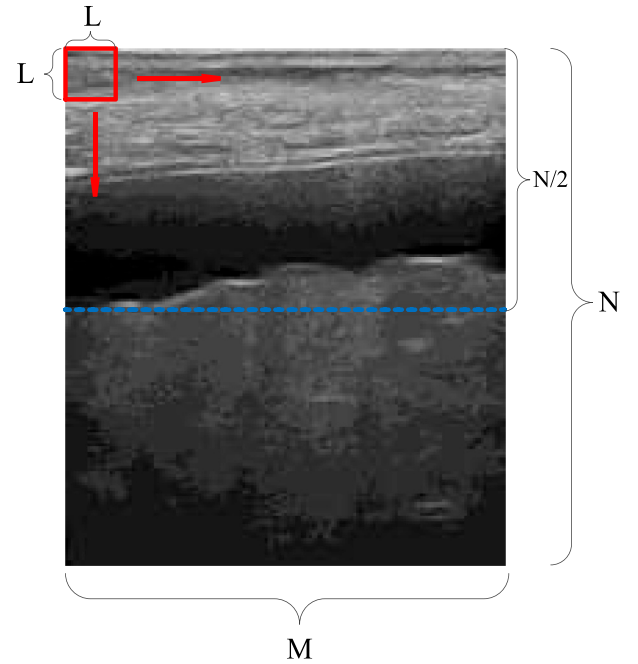

Fig. 3. Schematic diagram of sliding window detection.

algorithm is depicted in Fig. 3.

Assuming that the image size is $M \times N$, the size of the sliding window traversal area is $M \times N/2$; thus, when the window traverses one row or one column by the stride of L, the number of windows as shown in Eq. (1) are obtained. Therefore, when traversing the upper portion of the entire image, the total number of windows as shown in Eq. (2) are obtained.

$$S_r = M/L$$
$$S_c = (N/2)/L \tag{1}$$

$$S_a = S_r \times S_c \tag{2}$$

where S_r, S_c, and S_a represent the number of sliding windows in a row, a column, and the entire upper half of the image, respectively. Then, the average gray value of all the pixels in each window is calculated separately. It is determined that the window contains ascites if the average of the gray value of all pixels in the window is less than 60, which is the best threshold obtained from previous experimental verification. By calculating the average gray value of all windows, the number of sliding windows, S_f, containing ascites can be obtained. Determining the fixed threshold P through the experiment, it is possible to automatically

Table 1
Ultrasound image discrimination criteria for liver ascites.

Identification Criteria	Identification Result
$S_f/S_a \geq P$	Ascites image
$S_f/S_a < P$	No-ascites image

Table 2
Image processing fuzzy rules and their corresponding membership functions.

Fuzzy Rules	Membership Functions
If has a dark pixel, then makes it darker	$\mu_{dark}(z_0) = \begin{cases} 1, & v(z_0) \leq T_{dark} \\ \dfrac{T_{gray} - v(z_0)}{T_{gray} - T_{dark}}, & T_{dark} < v(z_0) \leq T_{gray} \\ 0, & v(z_0) > T_{gray} \end{cases}$
If a pixel is gray, then keeps it gray	$\mu_{gray}(z_0) = \begin{cases} \dfrac{v(z_0) - T_{gray}}{T_{gray} - T_{dark}}, & T_{dark} < v(z_0) < T_{gray} \\ \dfrac{T_{bright} - v(z_0)}{T_{bright} - T_{gray}}, & T_{gray} \leq v(z_0) < T_{bright} \\ 0, & v(z_0) \geq T_{bright} \;\; or \;\; v(z_0) \leq T_{dark} \end{cases}$
If has a bright pixel, then makes it brighter	$\mu_{bright}(z_0) = \begin{cases} 0, & v(z_0) \leq T_{gray} \\ \dfrac{v(z_0) - T_{gray}}{T_{bright} - T_{gray}}, & T_{gray} < v(z_0) \leq T_{bright} \\ 1, & v(z_0) > T_{bright} \end{cases}$

identify whether the ultrasound image has ascites by the discriminant standard presented in Table 1. Therefore, different parameters are set for ultrasound images with or without ascites to enable more efficient and accurate processing of an ultrasound image.

2.2.2. Ultrasound image enhancement with MDFS

The Gaussian blur [14,15] is first used for ultrasound images to eliminate noise. However, since the image information may be lost in the image denoising process, the denoised ultrasound image must be enhanced in the experiment for ensuring better detection of the liver capsule. Therefore, this paper proposes an enhanced method called MDFS which includes the enhancement of both multi-scale detail and fuzzy set.

(1) Multi-scale detail enhancement

In the multi-scale detail enhancement method [16,17], three differently blurred images are obtained by applying Gaussian kernels to the denoised ultrasound image I, as indicated in Eq. (3).

$$B_1 = G_1 * I, B_2 = G_2 * I, B_3 = G_3 - I \tag{3}$$

where G_1, G_2, G_3 are Gaussian kernels with standard deviations of 1, 2, and 20, respectively. Then, the fine detail D_1, the middle detail D_2, and the coarse detail D_3 are obtained using Eq. (4). Finally, different detail images are integrated into the final detail image by setting different weights, as shown in Eq. (5).

$$D_1 = I - B_1, D_2 = B_1 - B_2, D_3 = B_2 - B_3 \tag{4}$$

$$D' = (1 - \omega_1 \times \text{sgn}(D_1)) \times D_1 + \omega_2 \times D_2 + \omega_3 \times D_3 \tag{5}$$

$$I^* = I + D' \tag{6}$$

where ω_1, ω_2, ω_3 are fixed parameters with values of 0.5, 0.8, and 2, respectively in this paper. Then, the final detail D' is added to the denoised ultrasound image, as indicated Eq. (6), and the final detail enhanced image is obtained.

(2) Fuzzy set image enhancement

For the overall enhancement processing of the ultrasound image after detail enhancement, this paper uses the fuzzy set [18] to perform the gray level transformation. It involves making the dark pixels in the image become darker and the bright pixels become brighter, which is also suitable for the global enhancement processing of the liver ultrasound image and can better meet the needs of subsequent morphological processing. Before enhancement, the corresponding fuzzy rules and membership functions must be defined, which is done in Table 2.

For a pixel z_0 in the image, it is necessary to calculate the corresponding membership degree according to the fuzzy rule and the membership function to perform the blurring operation. Thereafter, the inverse defuzzification is performed according to Eq. (7) in order to obtain the pixel gray value of the processed result image. By traversing all the pixels of the entire ultrasound image and processing them in turn, the final overall enhanced image is obtained.

$$v_0 = \frac{\mu_{dark}(z_0) \times v_d + \mu_{gray}(z_0) \times v_g + \mu_{bright}(z_0) \times v_b}{\mu_{dark}(z_0) + \mu_{gray}(z_0) + \mu_{bright}(z_0)} \tag{7}$$
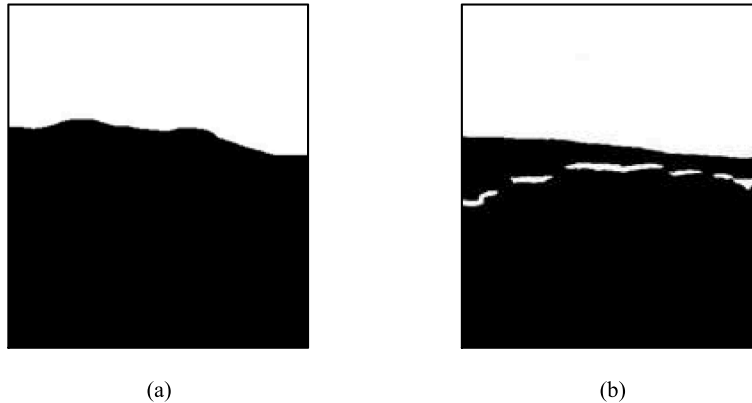

(a)   (b)

Fig. 4. Image processing results
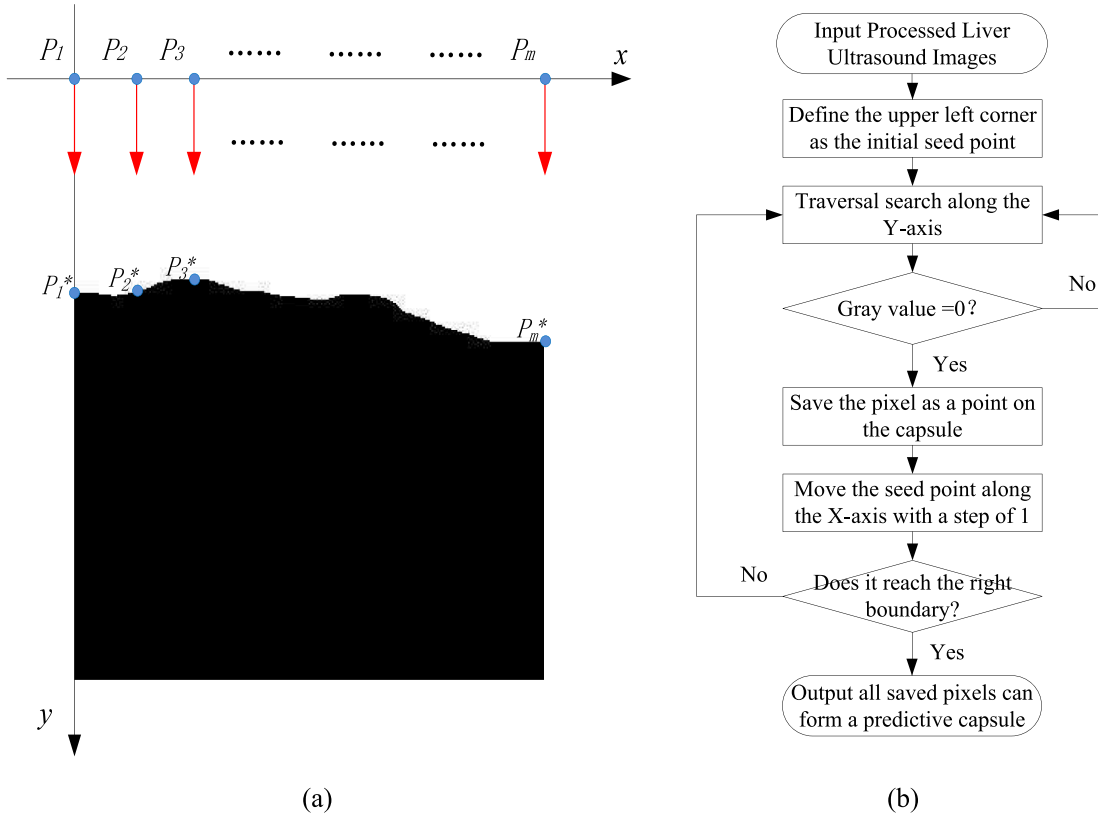(a) No-ascites image, (b) Ascites image.

Fig. 5. Introduce of traversal search algorithms for liver capsule of image without ascites.
(a) Algorithm diagrammatic sketch, (b) Algorithm flow chart.

where v_0 represents the gray value of the current pixel of the resulting image, v_d, v_g, and v_b are the single gray values of output, which are 0, 127, and 255, respectively; $\mu_{dark}(z_0)$, $\mu_{gray}(z_0)$, and $\mu_{bright}(z_0)$ represent three membership functions, respectively.

2.2.3. Structure segmentation with morphological processing

First, the adaptive threshold algorithm [19] is used to binarize the ultrasound image after denoising and enhancing it. Due to the structure of the liver and the irregular structural elements in the liver parenchyma, the image after binarization may contain a few isolated noise points. Therefore, before the morphological processing, it is necessary to set a certain threshold using the area method to eliminate the isolated noise, which is smaller than the threshold, thereby obtaining a more compact binary ultrasound image.

Further, in order to make the structure of liver image clearer and better satisfy the subsequent liver capsule detection algorithm, it is necessary to fill the clearances existing in the processed binary ultrasound image by using the morphological algorithm. Therefore, an independent connected domain [20] becomes visible in the muscle fat layer of the liver ultrasound image. In this paper, the image is processed by the morphological closing operation of Eq. (8), and the structural elements of varying sizes are used to process different ultrasound images with or without ascites.

$$A \bullet B = (A \oplus B)\Theta B \tag{8}$$

2.2.4. Predictive capsule extraction with the traversal search method

After processing these captured ultrasound images, the results of ultrasound images with ascites and no-ascites are depicted in Fig. 4. This paper mainly uses the traversal search method to detect and extract the liver capsule. However, a few discontinuous regions could be automatically fitted after previous processing. Therefore, the liver capsule

extracted by the algorithm can only be called the predictive capsule. Moreover, it is evident from Fig. 4 that the no-ascites ultrasound image contains only two connected domains after processing, while the ascites image contains multiple connected domains. Considering the difference between the two cases, this paper designs different detection and extraction schemes for predictive liver capsules.

(1) Predictive capsule extraction of no-ascites ultrasound images

Assuming that the image size is $m \times n$, the preprocessed image is placed in a novel coordinate system improved from the Cartesian coordinate system, the upper left corner of the graph is identical to the origin of the coordinate system, and the point on the predicted capsule is detected using the traversal search method [21]. The algorithm diagrammatic sketch is illustrated in Fig. 5(a).

First, the point P_1 of the upper left corner of the ultrasound image is selected and the search traverses in the positive direction of the Y-axis. When the pixel gray value is detected as 0, the search for the column is stopped and the pixel with a gray value of 0 is defined as the point P^*1 on the predictive capsule. Then, the point P_1 is shifted by one pixel from the initial position in the positive direction of the X-axis and P_1, P_2, P_3, …, Pm are sequentially obtained as starting points. M pixels which ultimately constitute the predictive liver capsule, P^*1, P^*2, P^*3, …, P^*m are obtained by repeating the above-described traverse search method. The algorithm flow chart is presented in Fig. 5(b).

(2) Predictive capsule extraction of ascites ultrasound images

It is evident from Fig. 4(b) that if the above method continues to be used for these processed ascites images, only the upper boundary of the ascites can be extracted, while the liver capsule is located in the lower boundary of the ascites region. Thus, it is necessary to improve the above
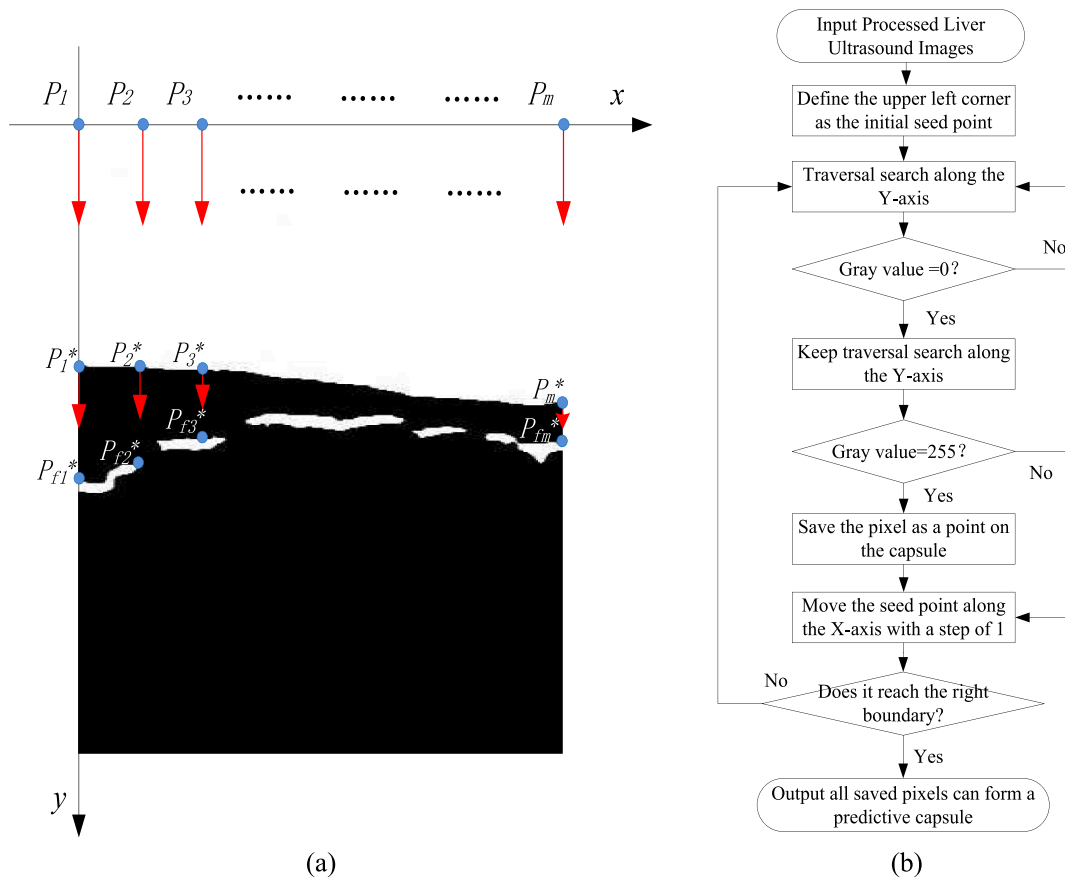
Fig. 6. Introduce of traversal search algorithms for liver capsule of image with ascites.
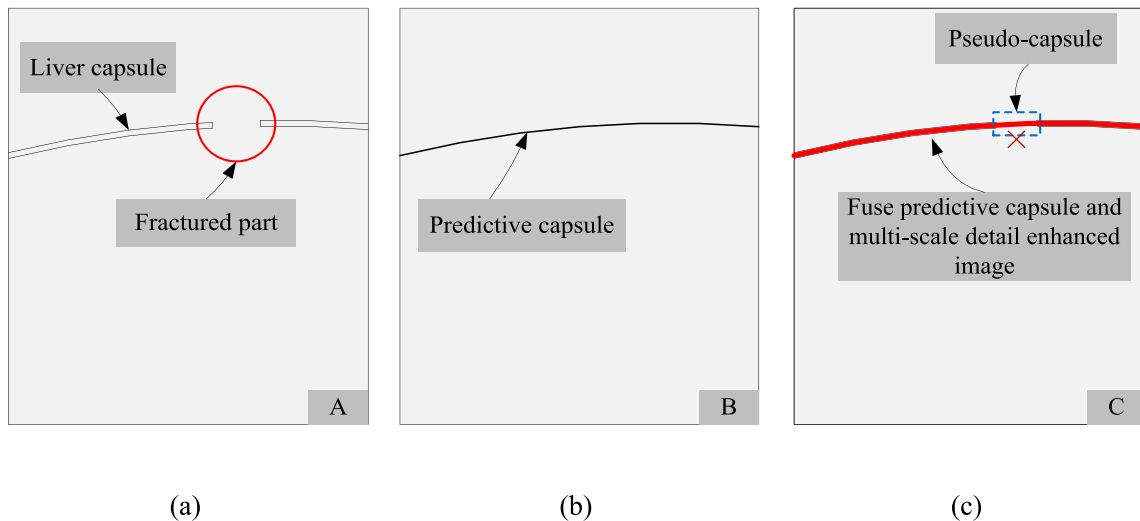(a) Algorithm diagrammatic sketch, (b) Algorithm flow chart.

Fig. 7. Diagrammatic sketch of real capsule processing.
(a) Multi-scale detail enhanced ultrasound image, (b) Predictive capsule image, (c) Fusion image of (a) and (b).

algorithm to achieve liver capsule extraction with ascites images.

Therefore, the traversal search is still performed for each column. When the pixel gray value is detected as 0, the search continues along the Y-axis until the pixel $P*_{f1}$ with a gray value of 255 is detected again; this pixel point can be defined as a point on the predictive capsule. Thereafter, all the retrieved pixels $P*_{f1}, P*_{f2}, P*_{f3}, …, P*_{fm}$ are finally saved to form a predictive capsule of a liver ultrasound image with

ascites. In addition, since there are break points in the liver capsule image with ascites, when the column of the broken portion is detected, the pixel with a gray value of 255 cannot be detected again after detecting a pixel with the gray value of 0. Therefore, this column is skipped and the traversal search for the next column continues. The diagrammatic sketch and flow chart of the algorithm are presented in Fig. 6.

2.3. Detection of real capsule using the gray difference method

The predictive capsule is effectively extracted by the traversal search algorithm, but the main problem in the predictive capsule is real liver capsule over-extraction. Consequently, certain "pseudo-capsule" of the discontinuous portion are extracted simultaneously with the real liver capsule. The core work of the extraction of the real liver capsule is to eliminate the "pseudo-capsule" portion from the predictive capsule. Therefore, this paper proposes the extraction of the real liver capsule through a method called the gray difference method [22], which is based on the predictive capsule.

The multi-scale detail enhanced liver ultrasound image is denoted as A; the extracted predicted capsule image is denoted as B; and the image obtained by fusing the dilated B with A is denoted as C. The diagrammatic sketch for this is presented in Fig. 7. Since the extracted predicted capsule is a single-pixel curve, the liver capsule in the actual ultrasound image has a certain thickness. Simultaneously, in order to avoid the position of the predicted capsule after fusion being in the same position of the liver capsule in the enhanced image, the extracted liver capsule must be dilated according to a certain size of the structural element, thereby ensuring that the effective areas after fusion are well overlapped.

It is assumed that the coordinates of pixels in the dilated predictive capsule region are (x,y), where $x \in (1, m)$. When the dilated predictive capsule is fused into the enhanced ultrasound image, the existence of the "pseudo capsule" can be searched from the first column one by one. According to the principle of Eq. (9), if the average gray value of one column in the enhanced ultrasound image, whose limits are similar with the y value range of the dilated predictive capsule, is larger than the threshold P, it will be proved that this column is the real liver capsule, thereby retaining the original pixel value of the same column in the predictive capsule. On the contrary, if the average value in the range is less than the threshold P, then the predicted capsule here is a "pseudo capsule". Therefore, the pixel value of this column in the predicted capsule must be set to 0. After traversing all the columns of the entire image, the remaining pixels in the predictive capsule will form the real liver capsule.

$$\begin{cases} G_3(i,j) = G_1(i,j) & G_2(x,y) \geq P \\ G_3(i,j) = 0 & G_2(x,y) < P \end{cases} \tag{9}$$

where $G_1(i,j)$ represents pixel gray value when the coordinates are (i,j) in the predictive capsule image, $G_2(x,y)$ represents pixel gray value when the coordinates are (x,y) in the enhanced ultrasound image, and $G_3(i,j)$ represents pixel gray value when the coordinates are (i,j) in the real capsule image.

2.4. Liver capsule feature extraction

With the development of cirrhosis, the liver capsule may be fractured, ladder-shaped, or jagged-shaped in morphology. Based on the characteristics of ultrasound medical imaging of the liver and the existing research, our experiment analyzed three kinds of morphological features containing smoothness and fluctuation based on predictive capsule and continuity based on real capsule. According to the three aspects, four geometric features are proposed to describe the changes in the liver capsule.

2.4.1. Continuity of the liver capsule

Continuity indicates the fracture condition of the liver capsule at different stages. In this paper, the line segments of the real capsule are detected, and the number of line segments (NoL) is calculated to indicate the continuity of the liver capsule.

$$NoL = k$$
$$L = \{l_i | i = 1, \ldots, k\} \tag{10}$$

$L = \{l_i | i = 1, \ldots, k|\}$ represents a set of lines that constitute the entire liver capsule.

2.4.2. Smoothness of the liver capsule

Smoothness mainly describes the overall trend of the liver capsule. We mainly analyze the variance of the sectional slopes (VoS) of the predictive capsule and coefficient of variation (CV) of slope difference between adjacent segments. In addition, due to the intermittent condition of the liver capsule under different stages, the same interval is used to split the line segments of the liver in order to avoid the impact of the discontinuous area on the feature analysis in this paper. The slopes of the small segments in each line segment are comprehensively analyzed to obtain overall smoothing characteristics.

(1) Variance of the sectional slope

Assuming that there are m line segments per liver capsule, where $m = (1, 2, \ldots, i)$, each line segment is divided into n small segments at the same interval with S pixels, where $n = (1, 2, \ldots, j)$, there are N_L small segments in the entire liver capsule image.

$$N_L = \sum_{i=1}^{m} n_i \tag{11}$$

where n_i represents the number of small segments in the i-th line segment. The slope of each small segment in each line segment is as indicated in Eq. (12), and the variance of the slope of the entire liver capsule is as indicated in Eq. (13).

$$K_{ij} = \frac{y_{E_{ij}} - y_{F_{ij}}}{x_{E_{ij}} - x_{F_{ij}}} \tag{12}$$

$$VoS = \frac{\sum_{i=1}^{m} \sum_{j=1}^{n} \left(K_{ij} - \overline{K} \right)^2}{N_L} \tag{13}$$

$$\overline{K} = \frac{\sum_{i=1}^{m} \sum_{j=1}^{n} K_{ij}}{N_L} \tag{14}$$

where K_{ij} represents the slope of the j-th small segment in the i-th line segment, (x_{Eij}, y_{Eij}) and (x_{Fij}, y_{Fij}) represent the coordinates of the first and last pixel points of each segment, respectively, and $\overline{K}$ represents the average slope of all small segments in the entire liver capsule.

(2) Coefficient of variation of slope difference between adjacent segments

The coefficient of variation is a statistic that measures the degree of variation in each observation in the indicator. Therefore, based on the slope of each small segment, the coefficient of variation of the slope difference (CV) of adjacent segments is analyzed to better describe the smoothness of the liver capsule. The coefficient of variation is presented in Eq. (15).

$$CV = \frac{STD_{K_d}}{\overline{K}_d} \tag{15}$$

where K_d represents the slope difference of adjacent small line segments, STD_{Kd} represents the standard deviation of the slope difference, and $\overline{K}_d$ represents the mean value of the slope difference.

2.4.3. Volatility of the liver capsule

Calculating the absolute value $|K_d|$ of the slope difference, K_d, between adjacent small segments based on the slope sequence composed of the slopes, K_{ij}, of small segments that are composed of S pixels. If $|K_d|$ is greater than 0.3, it is regarded as one fluctuation. The number of
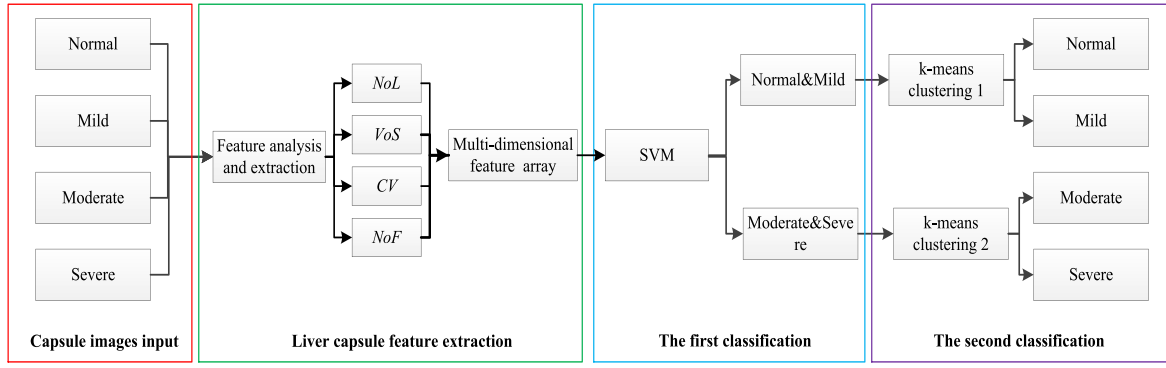
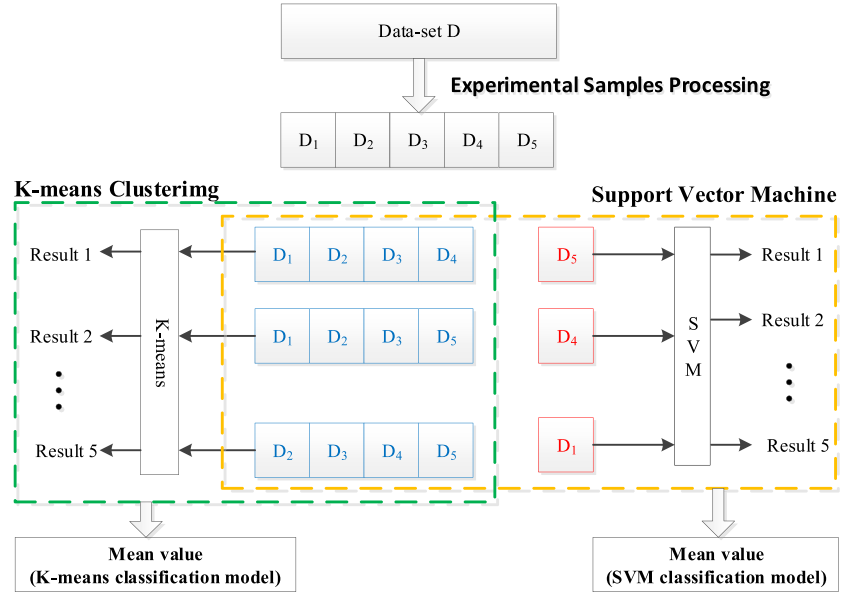**Fig. 8.** Flow chart of liver cirrhosis stage classification.

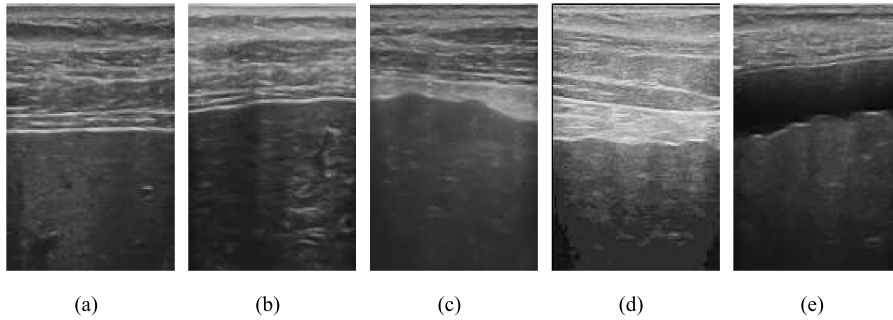**Fig. 9.** Diagrammatic sketch of ten-fold cross validation.

Fig. 10. Liver ultrasound images at different stages.
(a) Normal, (b) Mild, (c) Moderate, (d) Severe (no-ascites), (e) Severe (ascites).

fluctuations (*NoF*) of the entire curve indicates the fluctuation of the liver capsule, as indicated in Eq. (16), where the NoF_i is the fluctuation judgment criterion of adjacent small segments.
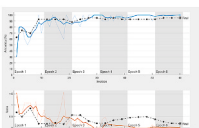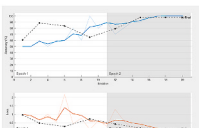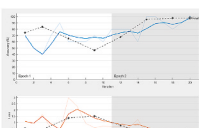
$$NoF = \sum_{i=1}^{N_L-1} NoF_i$$
$$NoF_i = \begin{cases} 1, & |K_d| \geq 0.3 \\ 0, & |K_d| < 0.3 \end{cases}$$

(16)

2.5. Establishment of a stage recognition model for liver cirrhosis

Because the morphological structure of the liver capsule is similar in normal and different cirrhosis stages, if a single machine learning model is adopted for the direct classification, it could result in recognition error and lower accuracy. At the same time, medical image samples are more precious and smaller in number. The choice of machine learning algorithms must ascribe priority to unsupervised learning algorithms that do

Table 3
Comparison of ascites detection accuracy.

Method	Recognition Accuracy /%	F1 Score	Process Image
AlexNet	95.35	0.850	
VGG-16	97.67	0.916	
VGG-19	97.67	0.916	
Ours	100.00	1.000	/

not require pre-training and supervised learning algorithms that are suitable for small samples. Therefore, considering the high similarity and the small number of samples, a two-stage classification model [23–25], as presented in Fig. 8 based on SVM with the RBF kernel function and k-means clustering is proposed in this paper.

The extracted liver capsule feature vector arrays are processed by the ten times five-fold cross-validation algorithm [26], as depicted in Fig. 9, and input into the SVM for training and recognition; then, the two major categories from the first classification model are obtained. Thereafter, each major category is also processed by the ten times five-fold cross-validation method, and the second classification results are obtained by k-means clustering. Consequently, four different stages are obtained through the two-stage classification model.

3. Results and discussion

A portion of the ultrasound images from each stage, which were part

of the experiment, are presented in Fig. 10. There is a difference in the morphology and structure of the liver capsule presented in the ultrasound images in a normal liver and in a liver affected by cirrhosis at various stages; thus, even in severe cases, there will be an ascites area and, thus, we were able to conduct the disease auxiliary diagnosis according to the extracted features. The liver capsule extraction, morphological feature analysis and disease classification were introduced with these images.

3.1. Analysis of the results of predictive liver capsule extraction

In this experiment, the first half of the entire ultrasound image was scanned by a 10×10 sliding window with 10 pixels as step size. When the average gray value of the pixel inside the window was less than 60, it was determined to contain the portion with ascites. By intercepting a number of ascites area windows in advance, the average value of the maximum gray value of all window pixels was obtained as the set threshold 60; thus, subsequent automatic recognition was performed according to this threshold. Experiments proved that when the ratio of the number of windows with ascites to the total windows was greater than 0.07, this image would be judged to be part of the ascites liver ultrasound image, otherwise, it was deemed part of the liver ultrasound image without ascites. Since convolution neural networks are popular for detecting such image information, we also adopted the transfer learning of a few deep learning models, including AlexNet, VGG-16 and VGG-19, for the detection of these ascites. In the experiments, the original data set was expanded to four times by data enhancement methods such as rotation, compression, and clipping; thereafter, the enhanced data set was divided into the training set and verification set in the ratio of 8:2, and input into deep learning models. The results of the experiment are presented in Table 3. A comparison of recognition accuracy and the F1 score reveals that our method proposed in this paper has a better effect; it also avoids the time taken for deep learning pre-training and requires lower equipment performance.

Further, the high-frequency noise information in the image was eliminated by Gaussian blurring and different parameters were set to process the liver ultrasound image with or without ascites. First, the denoised ultrasound image was enhanced using the MDFS algorithm. It is evident from Fig. 11 that the algorithm designed in this paper has a better effect compared with single global enhancement or single local
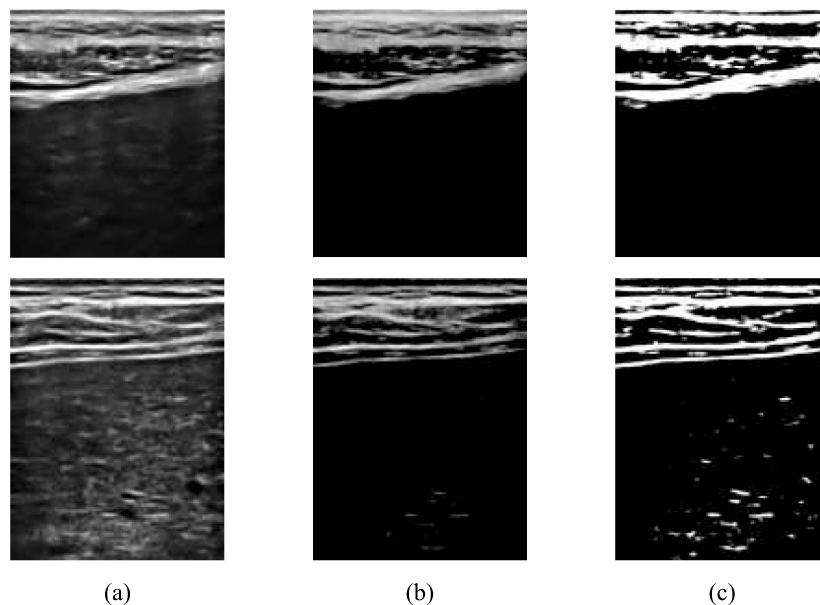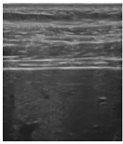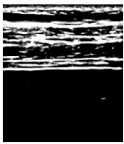

(a)   (b)   (c)
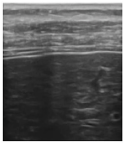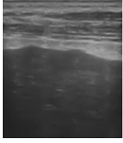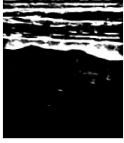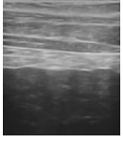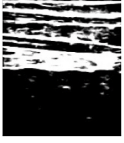
Fig. 11. Display of different image enhancement methods
(a) Multi-scale detail enhancement, (b) Fuzzy set image enhancement, (c) MDFS algorithm.

Table 4
Predictive liver capsule extraction process diagrams.

Stages	Gaussian Blur	MDFS Enhancement	Morphological Processing	Extracted Predictive Capsules
Normal				
Mild				
Moderate				
Severe (no-ascites)				
Severe (ascites)				
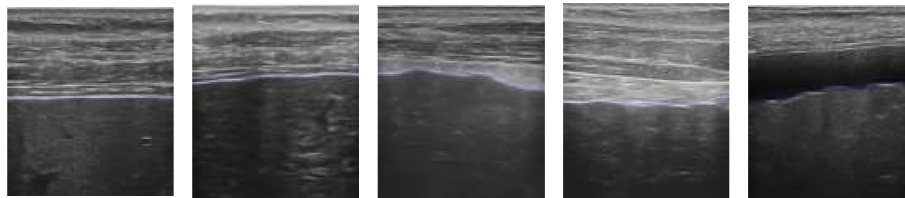
Fig. 12. Display of fusion images applied to the accuracy verification.

enhancement and the effect of these result images is better for the follow-up processing. Second, the morphological algorithm was used to make its structure clearer. The binary images of enhanced ultrasound images were obtained by the adaptive threshold algorithm, and the isolated noise points were eliminated. Then, these images were processed by the closed operation with a certain size of structural elements and the final binary ultrasound images with simple structures were obtained. Finally, the traversal search algorithm was utilized to extract the predictive liver capsule from the final binary ultrasound image.

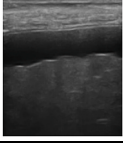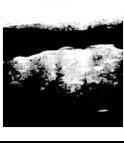However, the binary ultrasound image without ascites contained only two non-overlapping connected domains after processing, while the binary image with ascites had multiple connected domains. Therefore, the traversal search algorithm was adopted to detect the no-ascites liver capsule, while this algorithm was simultaneously improved for the ascites images. Consequently, automatic detection and extraction of the predictive liver capsule of all liver ultrasound images can be better realized. Taking the original liver ultrasound images of different stages presented in Fig. 10 as examples, the entire predictive capsule extraction experimental process images are presented in Table 4.

In order to verify the accuracy of the predictive liver capsule extraction, the extracted liver capsules were marked with blue, and the marked liver capsule images were fused with original ultrasound images, as presented in Fig. 12. It is evident that the extracted predictive

Table 5
Liver capsule detection accuracy.

Stages	Total	Success	Accuracy /%	Mean Accuracy/%
Normal	20	20	100.00	95.13
Mild	18	17	94.44	
Moderate	16	15	93.75	
Severe	13	12	92.31	

capsule could be well fused with the liver capsule region in the original ultrasound images. In addition, Table 5 indicates that the liver capsule extraction algorithm proposed in this paper could well realize the liver capsule extraction in various cirrhosis stages. The achieved accuracy with the experimental samples was 95.13%.

3.2. Analysis of the results of the real capsule extraction based on the predictive capsule

Because of the fitting of the fractured portions of the liver capsule by image processing, the predictive liver capsule extracted by the traversal search method is not a good representation of the real liver capsule. Therefore, the "pseudo capsule" portions were detected and excluded by
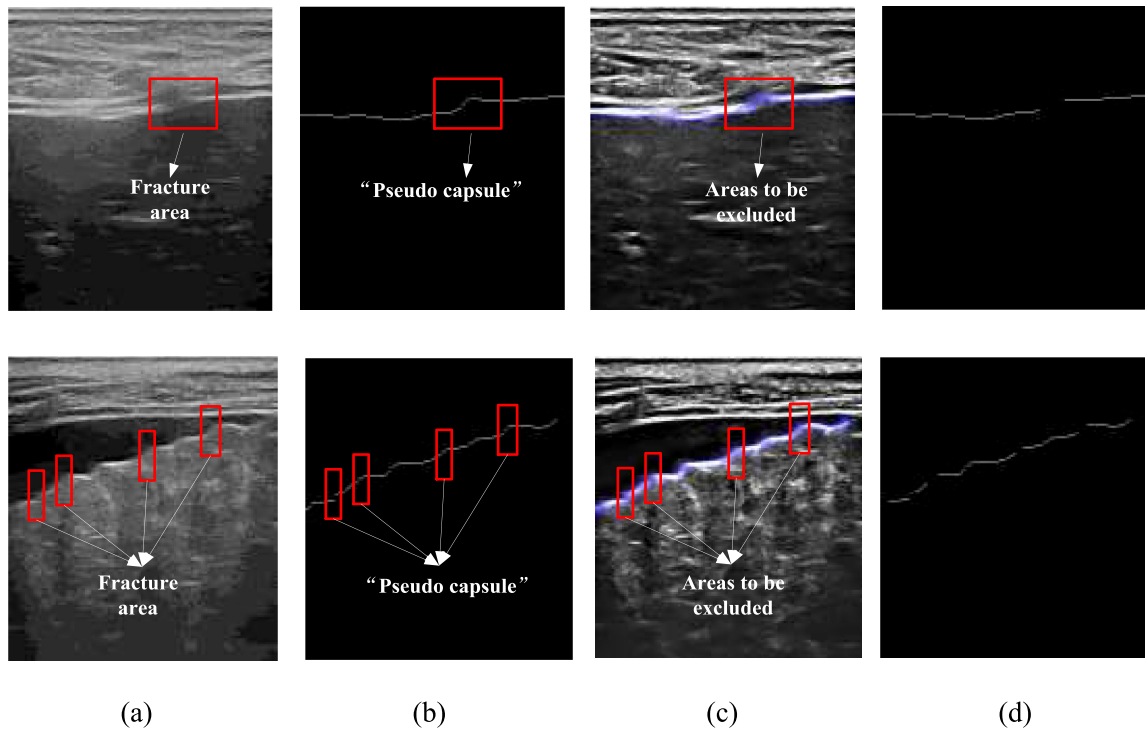
Fig. 13. Real liver capsule extraction process diagrams.
(a) Original images, (b) Predictive liver capsule images, (c) Fusion images, (d) Real liver capsule images.

the gray difference method based on the predictive capsule, and the real liver capsule was effectively extracted.

The extracted liver capsule was first dilated by a disk-shaped structural element of size of 10, so that the dilated liver capsule can better fit to the real liver capsule with the width in original images. In order to increase the contrast of the images and better realize the gray difference calculation of the liver capsule pixel, the ultrasound images enhanced with multiscale detail were fused with the dilated predictive liver capsule images. It was found that when the pixel gray value on the liver capsule of enhanced ultrasound image is less than 100, it indicates the position of the fracture of the real liver capsule, that is "pseudo capsule".

Therefore, in the experiment, when the average gray value of the enhanced ultrasound image was less than 100 within the coordinate range of the blue predictive capsule in the column, the gray value of the original predictive capsule in the same position as the column coordinate was defined as 0. After the gray difference of all the columns in the image was detected, the real liver capsule image was obtained from the predictive capsule. The entire extraction process is presented in Fig. 13. The final images of the real liver capsule in each liver stage is depicted in Fig. 14.

3.3. Analysis of the morphological features of the liver capsule

After the extraction of liver capsule, four morphological features of the liver capsule in four stages were calculated, as presented in Table 6, where the mean value is represented by *M*, and the standard deviation is represented by *S*. It is evident from Table 6 and Fig. 15 that the four features of different cirrhosis disease stages all have obvious differences from each other. Moreover, the standard deviations are relatively small and, thus, the features are relatively stable. Therefore, the four types of morphological features proposed in this paper can be used to describe and analyze the liver capsule and can be further utilized to assist in the diagnosis of liver disease at its various stages.

3.4. Classification and auxiliary diagnosis of cirrhosis

Through analysis of the feature data of the liver capsule, a two-stage classification model based on SVM and k-means clustering was developed in this paper. By classifying the original data twice, the accurate classification of a normal liver and the three stages of liver cirrhosis were finally enabled.

Moreover, because SVM and k-means clustering algorithm in this paper all were used for the two-classification in this paper, in order to evaluate the performance of this model, the *F*1 score indicated in *Eq.* (17) was adopted in this paper.

$$F1 = \frac{2 \times P \times R}{P + R} \tag{17}$$

$$P = \frac{TP}{TP + FP} \tag{18}$$

$$R = \frac{TP}{TP + FN} \tag{19}$$

where *P* is the precision; *R* is the recall; *TP*, *FN*, *FP*, and *TN* represent true positive, false negative, false positive, and true negative, respectively.

(1) The first classification

The first classification mainly divided the original data into two major categories. By analyzing the fluctuation and smoothness of the liver capsule, the three-dimensional feature vector array was constructed by *NoF*, *VoS*, and *CV*. Then, based on this three-dimensional feature vector array, the statistical analysis of three data sets including the normal-mild and moderate-severe, normal-moderate and mild-severe, and normal-severe and mild-moderate were conducted. The results are presented in Table 7. When $0.01 < P \leq 0.05$, it indicates a statistically significant level, and when $P \leq 0.01$, it indicates a notably statistically significant level. It is evident from the table that when the initial categories were selected as "normal-mild" and "moderate-
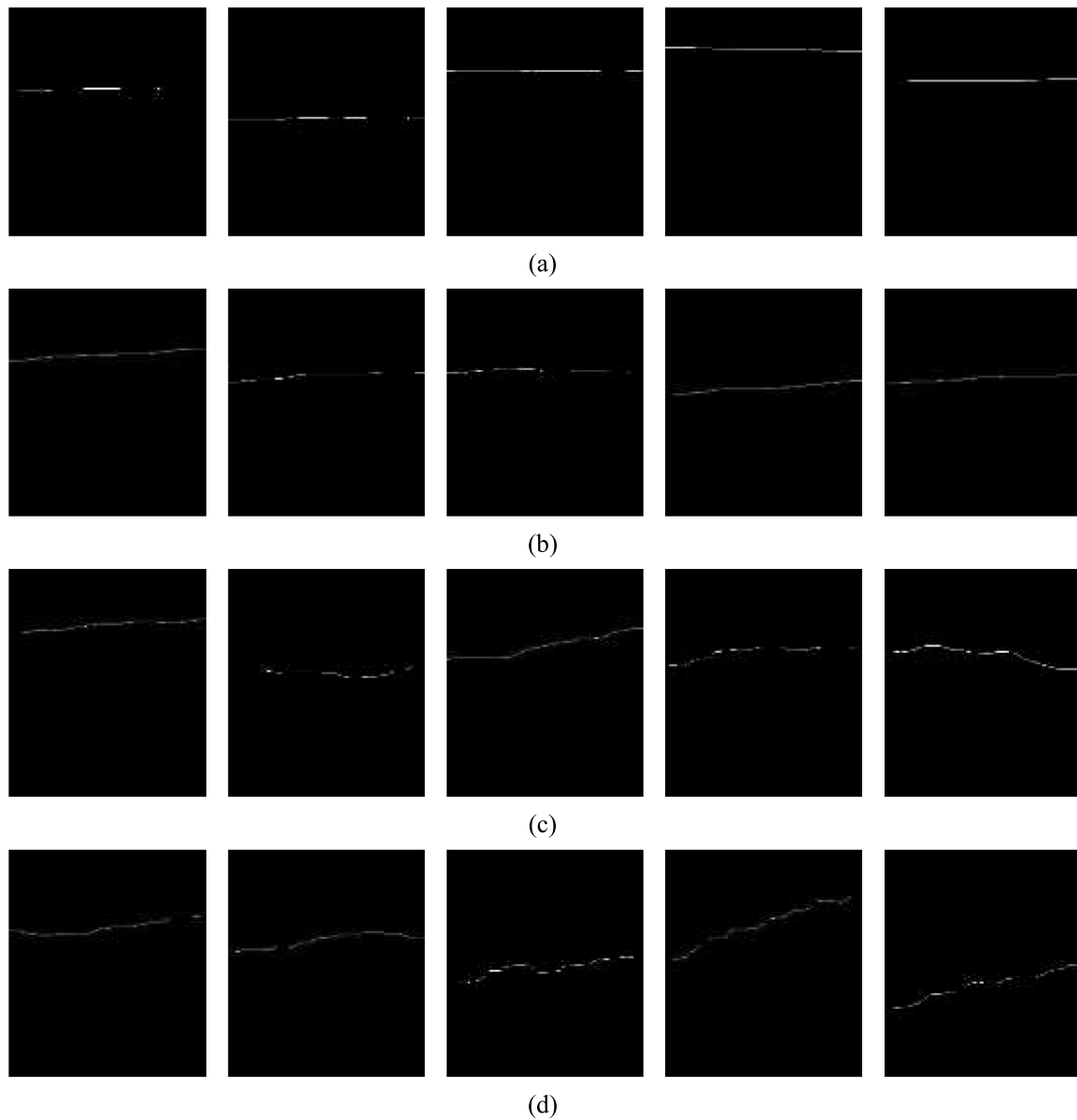
Fig. 14. Real liver capsule images in different stages.
(a) Normal, (b) Mild, (c) Moderate, (d) Severe.

Table 6
Liver capsule feature analysis results.

Features		Normal	Mild	Moderate	Severe
NoL	*M*	2.19	3.87	4.14	7.45
	S	0.98	1.50	1.95	2.16
NoF	*M*	0.63	2.00	7.23	15.00
	S	0.72	1.18	3.24	3.97
VoS	*M*	0.00	0.01	0.02	0.09
	S	0.00	0.00	0.01	0.08
CV	*M*	5.25	3.97	3.05	2.53
	S	1.12	0.68	0.67	0.91

severe", the feature analysis is notably statistically significant.

These three-dimensional feature vector arrays were put into the SVM for the first classification by means of the ten times five-fold cross-validation to realize the classification of "normal-mild" and "moderate-severe". The classification results are presented in Table 8, which indicates that the first classification has a great accuracy with 96.15% and

100% respectively, and the *F*1 scores are 0.972 and 0.967, respectively. The first classification also provided a better benchmark for the final classification of cirrhosis.

(2) The second classification

The first classification put the original data into two categories: the "normal-mild" category contained two sub-classes of normal and mild, and the "moderate-severe" category contained two sub-classes of moderate and severe. Due to the few experimental samples, the k-means classification model was used to cluster each major category to realize the second classification of four different stages.

For the category of "normal-mild", the *NoL* and *CV* were extracted to create a two-dimensional vector array by analyzing the continuity and smoothness of the liver capsule. It is evident from Tables 6 and 9 that there is a certain feature difference between the stages of normal and mild, and there is notable statistical significance. Therefore, the feature arrays were also processed by the ten times five-fold cross-validation. Using this method can roughly divided the data set into five parts, four
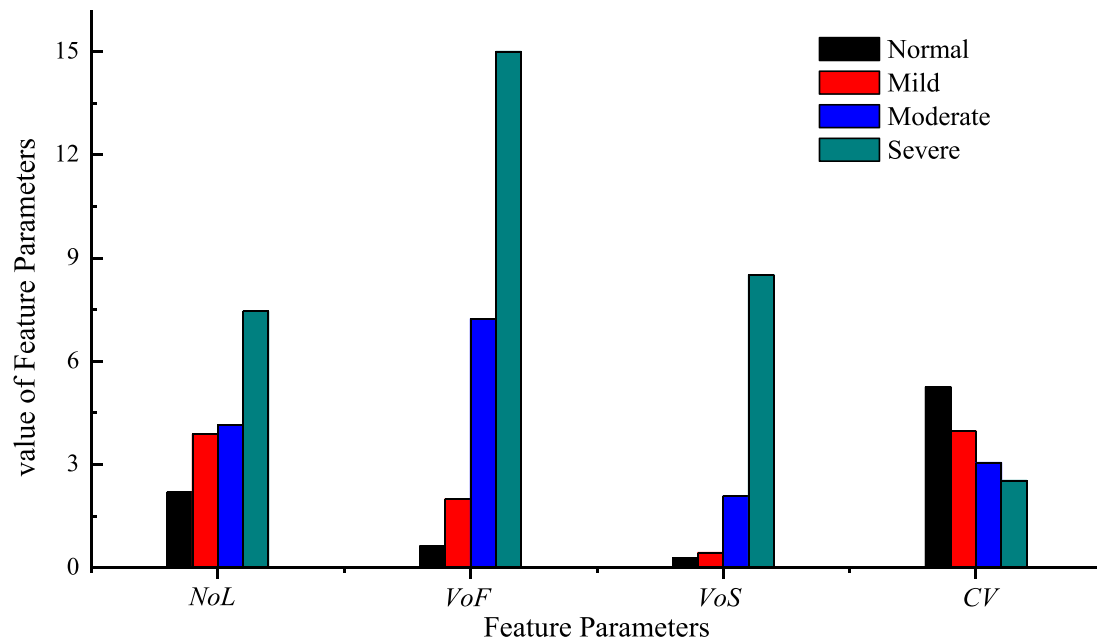
Fig. 15. Comparison of mean values of features in different stages.

Table 7
Features statistical analysis of two categories.

Categories		NoF	VoS	CV
P	Normal-Mild & Moderate-Severe	.000	.000	.000
	Normal-Moderate & Mild-Severe	.003	.011	.008
	Normal-Severe & Mild-Moderate	.339	.091	.085

Table 8
Results of the first classification.

Categories	Classification accuracy /%	F1 score
Normal-Mild	96.15 ± 0.01	0.972
Moderate-Severe	100 ± 0	0.967

Table 9
Features statistical analysis of normal and mild stages.

Features	NoL	CV
P	.001	.000

Table 10
Classification accuracy of normal and mild stages.

Categories	Classification accuracy /%	F1 score
Normal	96.25 ± 0.56	0.946
Mild	92.00 ± 1.03	0.938

Table 11
Features statistical analysis of moderate and severe stages.

Features	NoL	VoS
P	.001	.005

Table 12
Classification accuracy of moderate and severe stages.

Categories	Classification accuracy /%	F1 score
Moderate	89.23 ± 1.45	0.921
Severe	94.55 ± 1.21	0.910

Table 13
Accuracy of the two-stage recognition model.

Stages	Classification accuracy /%		
	First classification	Second classification	Final accuracy
Normal	96.15	96.25	92.54
Mild		92.00	88.46
Moderate	100.00	89.23	89.23
Severe		94.55	94.55

different portions were taken as input for the k-means clustering model each time and the experiment was repeated five times. Then, the average value was taken as the second classification accuracy of normal and mild stages. It is evident from Table 10 that the classification accuracy of normal and mild stages reached 96.25% and 92.00%, respectively, and the $F1$ scores are 0.946 and 0.938, respectively.

For the "moderate-severe" category, the NoL and VoS were extracted to create a two-dimensional vector array by analyzing the continuity and smoothness of the liver capsule and repeating the above ten times five-fold cross-validation experimental operation. It is evident from Tables 6 and 11 that there is also a certain feature difference between the stages of moderate and severe and there is notable statistical significance. In addition, it is evident from Table 12 that the second classification accuracy of moderate and severe stages reached 89.23% and 94.55%, respectively, and the $F1$ scores are 0.921 and 0.910, respectively.
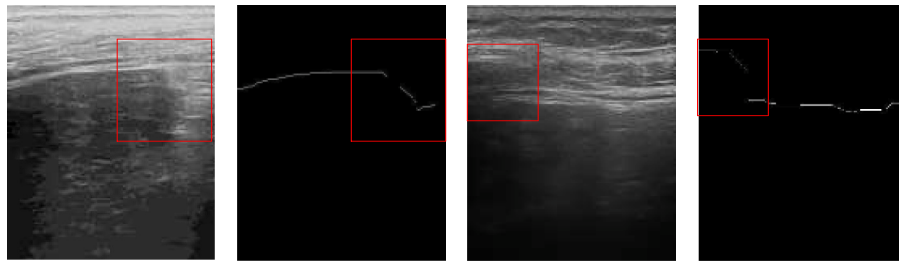
(3) Experimental error analysis

Fig. 16. Error recognition images display.

Table 14
Comparison of recognition accuracy with other methods.

Methods	Normal /%	Cirrhosis /%		
		Mild	Moderate	Severe
Lee et al. [6]	79.06	73.36	74.49	73.33
Virmani et al. [27]	74.39	77.32	73.66	78.81
Ribeiro et al. [28]	84.07	71.16	75.19	89.31
Kalyan et al. [29]	90.12	76.30	75.03	80.06
Liu et al. [9]	92.08	80.23	75.12	93.58
Zhao et al. [10]	92.50	74.71	70.08	86.17
Our method	**92.54**	**88.46**	**89.23**	**94.55**

It is evident from Table 13 that the cirrhosis-assisted diagnosis method via the morphological features of the liver capsule can obtain better classification accuracy in different stages with 92.54%, 88.46%, 89.23%, 94.55%, respectively; this may be helpful in assisting doctors in making a rapid clinical diagnosis.

It must be noted that there remained the phenomenon of classification error. The main reason for the classification error is that the imaging quality certain experimental samples is poor. Meanwhile, the main reason for the poor quality of ultrasound images is that during the acquisition process, due to the need to take into account the clarity of the liver parenchyma and the liver capsule simultaneously, the acquisition frequency has been slightly adjusted, thereby resulting in the liver parenchyma being too obvious and the liver capsule not being sufficiently clear. A few liver capsule areas presented in the red rectangular box of Fig. 16 are similar to the gray values that accord with liver parenchyma, which leads to errors in the detection and morphological feature extraction of the liver capsule, and eventually leads to the occurrence of recognition errors.

3.5. Comparison with other methods

When the classification accuracy of the proposed method was compared with other previous methods, in order to make the comparison highlight the advantages of this algorithm, two different comparison methods were adopted; the first is the utilization of different algorithms for different data sets and the second is the utilization of different algorithms for the same data set. The results are presented in Table 14. The method proposed in this paper provides a great improvement in the classification accuracy of different liver cirrhosis stages. Therefore, our method can be effectively applied to the clinical auxiliary diagnosis process of liver cirrhosis.

4. Conclusion

This paper proposed a novel method for accurate extraction of the liver capsule and auxiliary diagnosis of liver cirrhosis based on a high-frequency ultrasonic image. In this method, the predictive liver capsules are first extracted by the PLCD method. Then, according to the gray difference method, the real liver capsules are extracted. Finally, through the morphological feature analysis of the liver capsule, a two-stage classification system based on SVM and k-means clustering was designed for the auxiliary diagnosis of different cirrhosis stages.

The novel PLCD method proposed in this paper can accurately extract the predictive capsule which can reflect the actual location and trend of the liver capsule. The gray difference method proposed in this paper can accurately extract the real liver capsule, which reflects the real morphology. By combining three new morphological features of predictive capsule and one new morphological feature of the real capsule, the changes in the liver capsule can be more comprehensively described in different stages. Further, the experimental results also revealed that the proposed method can achieve effective auxiliary diagnosis of liver cirrhosis as well as provide reliable design ideas for analysis in other fields.

However, it is not only the liver capsule that can reflect a change in the stage of cirrhosis, but also the liver parenchyma. In order to better apply to the clinical auxiliary diagnosis, we aim to conduct further research on the liver parenchyma in the future. By combining the characteristics of the liver capsule and liver parenchyma, a more comprehensive description of a change in the stage of liver cirrhosis can be obtained, thereby enabling the diagnosis of the precise stage of liver cirrhosis in patients.

Declaration of competing interest

The authors declare no competing interests. We have received informed consent from each person to participate in our study, and been approved by the Changzheng Hospital Affiliated to Second Military Medical University to conduct this study.

References

[1] D. Schuppan, N.H. Afdhal, Liver cirrhosis, Lancet 371 (9615) (2008) 838–851, https://doi.org/10.1016/S0140-6736(08)60383-9.

[2] J. Peng, X. Peng, H. Tang, X. Li, R. Chen, Y. Li, T. Wang, S. Chen, K.K. Shung, Q. Zhou, Fabrication and performance of a miniaturized and integrated endoscope ultrasound convex array for digestive tract imaging, IEEE (Inst. Electr. Electron. Eng.) Trans. Biomed. Eng. 65 (1) (2018) 140–148, https://doi.org/10.1109/TBME.2017.2696560.

[3] M. Tanter, M. Fink, Ultrafast imaging in biomedical ultrasound, IEEE Trans. Ultrason. Ferroelectrics Freq. Contr. 61 (1) (2014) 102–119, https://doi.org/10.1109/TUFFC.2014.6689779.

[4] B.S. Garra, M.F. Insana, T.H. Shawker, R.F. Wagner, M. Bradford, M. Russell, Quantitative ultrasonic detection and classification of diffuse liver disease: comparison with human observer performance, Invest. Radiol. 24 (3) (1989) 196–203, https://doi.org/10.1097/00004424-198903000-00004.

[5] S.H. Wang, X. Liu, J. Zhao, J.L. Song, J.Q. Zhang, Y.Q. Chen, Learning to diagnose cirrhosis via combined liver capsule and parenchyma ultrasound image features, IEEE International Conference on Bioinformatics & Biomedicine (2017), https://doi.org/10.1109/BIBM.2016.7822627.

[6] W.L. Lee, Y.C. Chen, K.S. Hsieh, Ultrasonic liver tissues classification by fractal feature vector based on M-band wavelet transform, IEEE Trans. Med. Imag. 22 (3) (2003) 382–392, https://doi.org/10.1109/TMI.2003.809593.

[7] Z.P. Xu, X. Liu, X.E. Cheng, J. Lin, J.Q. Zhang, Diagnosis of cirrhosis stage via deep neural network, in: 2017 IEEE International Conference on Bioinformatics and Biomedicine (BIBM), IEEE Computer Society, 2017, https://doi.org/10.1109/BIBM.2017.8217748.

[8] X. Liu, J.L. Song, J.W. Zhao, Y.Q. Chen, J.Q. Zhang, Extracting and describing liver capsule contour in high-frequency ultrasound image for early HBV cirrhosis diagnosis, in: 2016 IEEE International Conference on Multimedia and Expo (ICME), 2016, https://doi.org/10.1109/ICME.2016.7552977.

[9] X. Liu, J.L. Song, S.H. Wang, J.W. Zhao, Y.Q. Chen, Learning to diagnose cirrhosis with liver capsule guided ultrasound image classification, Sensors 17 (1) (2017) 149, https://doi.org/10.3390/s17010149.

[10] J. Zhao, S.H. Wang, X. Liu, Y. Liu, Y.Q. Chen, Early diagnosis of cirrhosis via automatic location and geometric description of liver capsule, Vis. Comput. 34 (12) (2018) 1677–1689, https://doi.org/10.1007/s00371-017-1441-2.

[11] G.X. Fu, X. Liu, J.L. Song, J.W. Zhao, A liver capsule extraction algorithm based on high frequency ultrasound images, Electronic Science and Technology 11 (2019) 33–37, https://doi.org/10.16180/j.cnki.issn1007-7820.2019.11.007.

[12] B. Erwin, Diagnosis and therapy of ascites in liver cirrhosis, World J. Gastroenterol. 17 (10) (2011) 1237–1248, https://doi.org/10.3748/wjg.v17.i10.1237.

[13] L. Yang, G. Yang, Y. Yin, R. Xiao, Sliding window-based region of interest extraction for finger vein images, Sensors 13 (3) (2013) 3799–3815, https://doi.org/10.3390/s130303799.

[14] E.S. Gedraite, M. Hadad, Investigation on the effect of a Gaussian Blur in image filtering and segmentation, Elmar Proceedings, Zadar, Croatia (2011) 393–396.

[15] X.W. Liu, C.Y. Liu, An optional gauss filter image denoising method based on difference image fast fuzzy clustering, Appl. Mech. Mater. 411–414 (2013) 1348–1352. https://doi.org/10.4028/www.scientific.net/AMM.411-414.1348.

[16] H. Zhu, X.M. Tang, J.F. Xie, W.D. Song, Spatio-temporal super-resolution reconstruction of remote-sensing images based on adaptive multi-scale detail enhancement, Sensors 18 (2) (2018) 498, https://doi.org/10.3390/s18020498.

[17] Y. Kim, Y.J. Koh, C. Lee, S. Kim, C.S. Kim, Dark image enhancement based on pairwise target contrast and multi-scale detail boosting, in: IEEE International Conference on Image Processing, 2015, pp. 1404–1408. Canada.

[18] S.A. Pal, R.A. King, Image enhancement using smoothing with fuzzy sets, IEEE Transactions on Systems Man & Cybernetics 11 (7) (1981) 494–501, https://doi.org/10.1109/TSMC.1981.4308726.

[19] N. Ostu, A threshold selection method from gray-histogram, IEEE Transactions on Systems, Man, and Cybernetics 9 (2007) 62–66, https://doi.org/10.1109/TSMC.1979.4310076.

[20] W.Y. Xing, B.J. Xin, N. Deng, Y. Chen, Z.Y. Zhang, A novel digital analysis method for measuring and identifying of wool and cashmere fibers, Measurement 132 (2019) 11–21, https://doi.org/10.1016/j.measurement.2018.09.032.

[21] M. Yi, A ROI Marker Matching Method Based on Intravascular Ultrasound Image. CN 104537645 A[P], 2015.

[22] H. Zou, J.Y. Meng, H.Z. Shu, L.M. Luo, A fast and effective gray level interpolation of medical images, Journal of Biomedical Engineering Research 22 (4) (2003) 8–11, https://doi.org/10.19529/j.cnki.1672-6278.2003.04.003.

[23] C. Mi, J. Wang, W.J. Mi, Y.F. Huang, Z.W. Zhang, Y.S. Yang, J. Jiang, P. Octavian, Research on regional clustering and two-stage SVM method for container truck recognition, Discrete Continuous Dyn. Syst. - Ser. S 12 (4–5) (2019) 1117–1133, https://doi.org/10.3934/dcdss.2019077.

[24] M. Pal, G.M. Foody, Feature selection for classification of hyperspectral data by SVM, IEEE Trans. Geosci. Rem. Sens. 48 (5) (2010) 2297–2307, https://doi.org/10.1109/tgrs.2009.2039484.

[25] C. Selvi, E. Sivasankar, A novel Adaptive Genetic Neural Network (AGNN) model for recommender systems using modified k-means clustering approach, Multimed. Tool. Appl. 78 (11) (2019) 14303–14330, https://doi.org/10.1007/s11042-018-6790-y.

[26] W.Y. Xing, N. Deng, B.J. Xin, Y. Chen, Z.Y. Zhang, Investigation of a novel automatic microscopic image-based method for the recognition of animal fibers based on Wavelet and Markov Random Field, Micron 119 (2019) 88–97, https://doi.org/10.1016/j.micron.2019.01.009.

[27] J. Virmani, V. Kumar, N. Kalra, N. Khandelwal, Prediction of cirrhosis from liver ultrasound B-mode images based on Laws' masks analysis, Int. J. Converg. Comput. 1 (1) (2013) 19–37, https://doi.org/10.1109/ICIIP.2011.6108894.

[28] R. Ribeiro, R.T. Marinho, J. Suri, Ultrasound liver surface and textural characterization for the detection of liver cirrhosis, Abdomen and Thoracic Imaging 6 (2013) 145–168, https://doi.org/10.1007/978-1-4614-8498-1_6.

[29] K. Kalyan, B. Jakhia, R.D. Lele, M. Joshi, A. Chowdhary, Artificial neural network application in the diagnosis of disease conditions with liver ultrasound images, Advances in Bioinformatics (2014) 1–14, https://doi.org/10.1155/2014/708279, 2014.